





Two novel heteropolymer-forming proteins maintain the multicellular shape of the cyanobacterium *Anabaena* sp. PCC 7120

Benjamin L. Springstein¹ , Dennis J. Nürnberg^{2,*} , Christian Woehle^{1,†}, Julia Weissenbach^{1,‡}, Marius L. Theune¹, Andreas O. Helbig³, Iris Maldener⁴, Tal Dagan¹  and Karina Stucken⁵ 

1 Institute of General Microbiology, University of Kiel, Germany

2 Department of Life Sciences, Imperial College, London, UK

3 AG Proteomics & Bioanalytics, Institute for Experimental Medicine, Christian-Albrechts-Universität zu Kiel, Germany

4 Interfaculty Institute of Microbiology and Infection Medicine Tübingen/Organismic Interactions, University of Tübingen, Germany

5 Department of Food Engineering, University of La Serena, Chile

Keywords

Anabaena; cyanobacteria; filaments; heteropolymer; multicellular shape

Correspondence

B. L. Springstein, Department of Microbiology, Blavatnik Institute, Harvard Medical School, 4 Blackfan Cir, Boston, MA, 02115, USA

Tel: +1 857 225 4160

E-mail:

benjamin_springstein@hms.harvard.edu and

K. Stucken, Department of Food Engineering, University of La Serena, Av. Raúl Bitrán N°1305, La Serena, 1720010, Chile

Tel: +56 51 2204397

E-mail: kstucken@userena.cl

Present address

* Institute of Experimental Physics, Free University of Berlin, Berlin, Germany

† Max Planck-Genome-Centre Cologne, Max Planck Institute for Plant Breeding Research, Cologne, Germany

‡ Faculty of Biology, Technion-Israel Institute of Technology, Haifa, Israel

(Received 9 June 2020, revised 29 October 2020, accepted 13 November 2020)

doi:10.1111/febs.15630

Polymerizing and filament-forming proteins are instrumental for numerous cellular processes such as cell division and growth. Their function in stabilization and localization of protein complexes and replicons is achieved by a filamentous structure. Known filamentous proteins assemble into homopolymers consisting of single subunits – for example, MreB and FtsZ in bacteria – or heteropolymers that are composed of two subunits, for example, keratin and α/β tubulin in eukaryotes. Here, we describe two novel coiled-coil-rich proteins (CCRPs) in the filament-forming cyanobacterium *Anabaena* sp. PCC 7120 (hereafter *Anabaena*) that assemble into a heteropolymer and function in the maintenance of the *Anabaena* multicellular shape (termed trichome). The two CCRPs – Alr4504 and Alr4505 (named ZicK and ZacK) – are strictly interdependent for the assembly of protein filaments *in vivo* and polymerize nucleotide independently *in vitro*, similar to known intermediate filament (IF) proteins. A $\Delta zicK\Delta zacK$ double mutant is characterized by a zigzagged cell arrangement and hence a loss of the typical linear *Anabaena* trichome shape. ZicK and ZacK interact with themselves, with each other, with the elongasome protein MreB, the septal junction protein SepJ and the divisome associate septal protein SepI. Our results suggest that ZicK and ZacK function in cooperation with SepJ and MreB to stabilize the *Anabaena* trichome and are likely essential for the manifestation of the multicellular shape in *Anabaena*. Our study reveals the presence of filament-forming IF-like proteins whose function is achieved through the formation of heteropolymers in cyanobacteria.

Abbreviations

CC, coiled-coil; CCRP, coiled-coil-rich proteins; CDF, cumulative distribution function; CSB, conserved syntenic blocks; DAPI, 4',6-diamidino-2-phenylindole; FRAP, fluorescence recovery after photobleaching; PBP, penicillin-binding protein; PG, peptidoglycan; Van-FL, BODIPYTM FL vancomycin.

Introduction

Cytoskeletal proteins that polymerize to form protein filaments are paramount in bacterial cell biology where they play a role in cell division, alignment of bacterial microcompartments (BMCs), chromosome and plasmid segregation, organization of cell polarity and the determination of cell shape [1]. For example, FtsZ [2], the prokaryotic homolog to the eukaryotic tubulin [3], is a main component of the divisome [4], a multiprotein complex that governs cell division in bacteria and self-assembles into a proteinaceous ring (called Z-ring) at the midcell position [5]. Another key bacterial cytoskeletal protein is MreB [6], which is a homolog of the eukaryotic actin [2,7] and a crucial component of the multiprotein complexes termed the elongasome. This complex modulates cell elongation in many rod-shaped bacteria through regulating peptidoglycan (PG) biogenesis [8]. Both, FtsZ and MreB monomers assemble into filamentous strands (protofilaments), consisting of only one type of monomer, termed homopolymers [1]. The cell division in prokaryotes markedly contrasts the division of plastid organelles in photosynthetic eukaryotes that are of cyanobacterial origin [9]. Cell division in plastids is dependent on the cooperative function and heteropolymerization of two FtsZ homologs, FtsZ1 and FtsZ2 in the green lineages and FtsZA and FtsZB in the red lineage. However, each FtsZ homolog is also self-sufficient to form homopolymers (reviewed by [10]). In contrast, a likely horizontally transferred pair of tubulin homologs, BtubA and BtubB from *Prothescobacter* spp., exclusively assembles into heteropolymers *in vitro* [11], revealing similar properties than eukaryotic microtubules that are heteropolymers composed of α and β tubulin monomers [12]. Eukaryotic IF proteins, despite sharing substantially the same building blocks and a high degree of coiled-coil (CC) domains [13], which are considered excellent mediators of protein–protein interactions [14], only form heteropolymers with a subset of other IF proteins within their same assembly group but otherwise form obligate homopolymers [15].

Polymer-forming coiled-coil-rich proteins (CCRPs) have been shown to play a role also in multicellularity traits in myxobacteria and actinomycetes (reviewed by [1,16]). Similar to eukaryotic IFs [13], many bacterial CCRPs perform cytoskeletal functions through their ability to self-assemble into filaments *in vivo* and *in vitro* in a self-sufficient and cofactor independent manner [17–20]. The CCRP Crescentin determines the *Caulobacter crescentus* typical curved morphology by aligning to the inner cell curvature and exuding local mechanical constraints on the PG biosynthesis, likely

through cooperation with MreB [17,21]. In analogy to eukaryotic IF proteins, Crescentin assembles into straight protein filaments with a width of 10 nm and displays a similar domain organization [17]. However, while Crescentin is often considered a prokaryotic homologue to eukaryotic IF proteins, its restricted distribution to only one identified organism questions real homologous relationships and rather suggests that it was acquired by horizontal gene transfer [22]. Multicellular actinobacteria, such as *Streptomyces* spp., grow by building new cell wall (i.e., PG) only at the cell poles, independent of MreB [23], a striking different cell growth than in most other bacteria [24]. This characteristic polar growth mode is organized by a cytoskeletal network of at least three CCRPs – DivIVA, Scy and FilP – that directly interact with each other to form the polarisome [18]. FilP and Scy independently self-assemble into filaments *in vitro* [18,25], thereby fulfilling major IF-like criteria [1]. *In vivo*, however, Scy does not form filaments and instead accumulates as foci at future branching points [18], while FilP localizes as gradient-like caudates at the hyphal tips [26], instead of forming distinct filaments as observed for Crescentin [17].

Among prokaryotes, cyanobacteria exhibit the largest morphological diversity, comprising unicellular species as well as complex cell-differentiating multicellular species [27]. For the model multicellular cyanobacterium *Anabaena*, it is imperative to form stable trichomes in order to cope with external influences such as shearing stress [28,29]. Under nitrogen-depleted growth conditions, *Anabaena* develops specialized cell types for nitrogen fixation (heterocysts), which are evenly spaced among the *Anabaena* trichome and provide other vegetative cells with fixed nitrogen compounds like glutamine [30]. In *Anabaena*, proteinaceous cell-joining structures that allow intercellular transport (i.e., cell–cell communication) and function by gating are termed septal junctions (analogous to eukaryotic gap junctions; [31,32]). Septal junctions consist of several structural elements, an intracellular cap, a plug inside the cytoplasmic membrane formed by the septal junction protein FraD and a tube traversing the septum through nanopores in the peptidoglycan [31]. The correct positioning of the septal protein SepJ, which is involved in septum maturation and filament stability, among others, depends on the FtsZ-driven divisome component FtsQ [33], which links the early and late assembly components of the divisome [34]. FtsZ was shown to be essential for *Anabaena* viability and to assemble in a typical Z-ring structure at future septum sites in vegetative cells while being downregulated in heterocysts [35–37]. In

contrast, MreB is dispensable for *Anabaena* viability but determines its typical cylindrical cell shape, since $\Delta mreB$ mutant cells display a pronounced rounded and swollen morphotype. This cell swelling, however, does not affect chromosome segregation, which was found to be governed, at least in part, by random segregation in *Anabaena* [38]. Maintenance of the cylindrical cell shape is furthermore dependent on a class B penicillin-binding protein (PBP) [39] and AmiC-type cell wall amidases in *Anabaena* [40,41], suggesting that loss of normal cell shape is commonly associated with defects in PG biogenesis.

In this work, we aimed to identify proteins that play a role in cyanobacterial morphology and multicellularity. Searching for IF-like CCRPs, we identified two novel CCRPs in *Anabaena* that are capable of assembly exclusively into a heteropolymer *in vitro* and *in vivo* and that have a putative role in the *Anabaena* linear trichome shape.

Results

CCRPs ZicK and ZacK from *Anabaena* are conserved in cyanobacteria

A computational survey of the *Anabaena* genome for protein-coding genes containing a high coiled-coil content [42] revealed two CCRPs Alr4504 and Alr4505; here, we term the two CCRPs ZicK and ZacK, respectively (*i.e.*, zig and zag in German). ZicK is predicted to contain five distinct coiled-coil (CC) domains, while ZacK has four CC domains (Fig. 1A; File S1). Using PSORTb (v.3.0.2), both ZicK and ZacK are predicted to be cytoplasmic proteins, which is corroborated by the absence of detectable transmembrane domains (predicted using TMHMM v. 2.0). Since both proteins (and their homologs) are annotated as hypothetical proteins (File S2), we validated their transcription under standard (BG11) and diazotrophic (BG11₀) growth conditions (Fig. S1B,C). The genomic neighbourhood of *zicK* and *zacK* motivated us to test for a common transcriptional regulation of both genes (*i.e.*, an operon structure); however, we did not identify a common transcript (using RT-PCR; Fig. S1A,B). Searching for known proteins sharing structural similarities to ZicK/ZacK using I-TASSER revealed structural similarities between ZicK and the eukaryotic cytolinker protein plectin, and of ZacK with the cell division protein EzrA, a predicted structural similarity that was previously associated with other bacterial CCRPs, including Crescentin, HmpF_{Syn} and HmpF_{Syc} [42]. Further annotation using the NCBI conserved domain search [43] showed that ZicK and ZacK contain ‘structural maintenance of chromosomes’

(SMC) domains (Fig. 1B), similarly to what we previously identified in other self-polymerizing cyanobacterial CCRPs [42]. A search for ZicK/ZacK homologs by sequence similarity revealed that they are absent in picocyanobacteria (*i.e.*, *Synechococcus/Prochlorococcus*) and generally rare in unicellular cyanobacteria. Otherwise, about 50% of the examined 168 cyanobacterial genomes have homologs for the two genes (Fig. 1C and File S2). Several heterocystous cyanobacteria lacking ZicK/ZacK homologs are characterized by a reduced genome (*e.g.*, *Nostoc azollae* PCC 0708 and *Richelia intracellularis*). Additionally, *Chlorogloeopsis* spp. that forms multiserial filaments is lacking the homologs and several strains of *Fischerella* spp., which form true branching filaments, harbour only a ZacK homolog. The protein sequence of ZicK and ZacK homologs is well conserved, with about 55% amino acids identity among the homologs. The number of CC domains, however, differ among ZicK and ZacK homologs: between 3–6 CC domains in ZicK homologs, and 3–10 domains in ZacK homologs (File S1). Notably, ZicK and ZacK are neighbours in 53 out of 72 genomes; both proteins and their genomic neighbourhood are highly conserved among heterocystous cyanobacteria (Fig. 1C,D).

ZicK and ZacK are interdependent for polymerization *in vitro*

As a prerequisite for proteins to be considered as IF-like proteins, it is imperative for them to be able to self-interact *in vivo* and to polymerize into long protein filaments *in vitro* [1]. To investigate the *in vitro* polymerization properties of ZicK and ZacK, we employed an *in vitro* polymerization assay that we previously established to test CCRPs’ polymerization properties [42]. As a positive control for our approach, we used Crescentin (Fig. 1A), which formed an extensive filamentous network in our *in vitro* assay (Fig. S2). As negative controls, we included empty vector-carrying *Escherichia coli* cells, GroEL1.2 from *Chlorogloeopsis fritschii* PCC 6912 (known to form oligomers [44]) and the highly soluble maltose-binding protein (MBP), all of which were tested negative for filament formation *in vitro* using our approach (Fig. S2). Purified ZicK protein formed into amorphous, nonfilamentous protein aggregates while for ZacK low levels of aggregated sheet-like structures could be observed (Fig. 2A). However, the vast majority of ZacK protein precipitated into clumps of aggregates upon renaturation, which resembled the structures observed for GroEL1.2, suggesting that ZacK has only a partial capacity to self-polymerize or, more likely, is highly unstable on its own *in vitro*. Inspired by the close

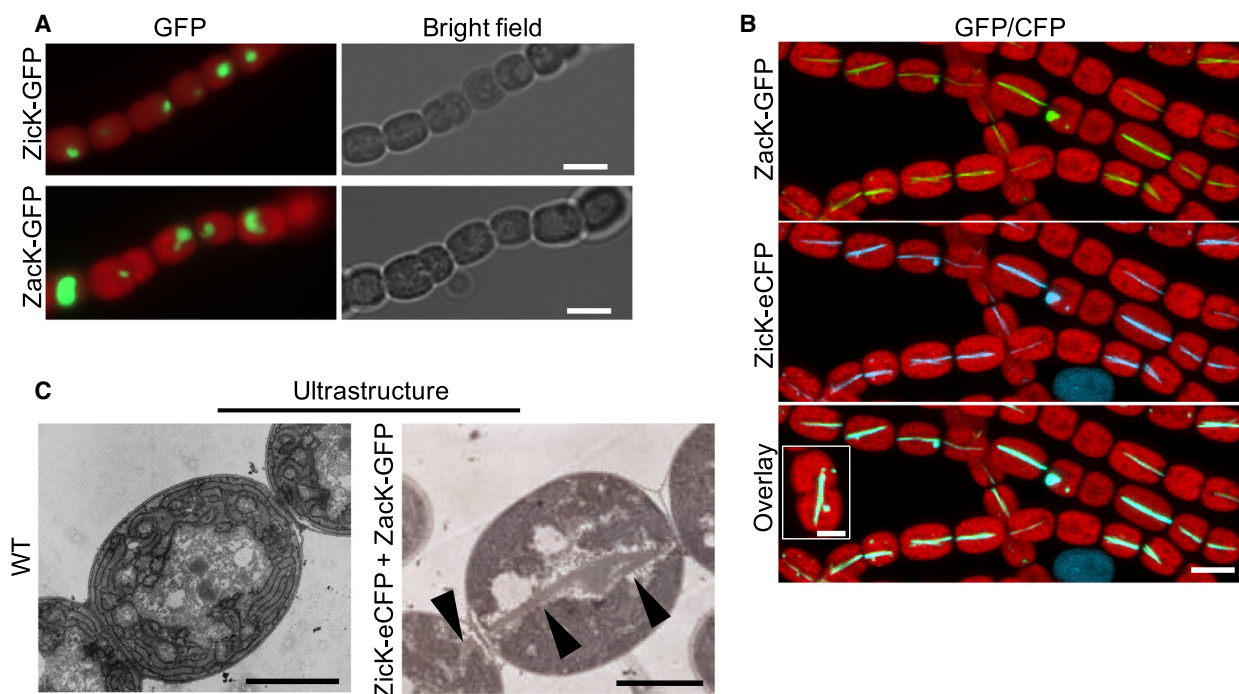


Fig. 3. ZicK and ZacK form a heteropolymer *in vivo*. (A, B) Merged GFP or eCFP-fluorescence and chlorophyll autofluorescence (red) and bright-field micrographs of *Anabaena* WT cells expressing (A) ZicK-GFP, ZacK-GFP or (B) co-expressing ZicK-eCFP and ZacK-GFP from P_{petE} . (B) Inlay shows that ZicK/ZacK filaments only cross not yet fully divided cells. (A, B) Results show representative figures from three independent experiments. Scale bars: (A, B) 5 μm , (B) inlay 2.5 μm . Notably, overexpression of ZicK-eCFP and ZacK-GFP does not lead to morphological alterations in *Anabaena*; however, it is likely that the fluorescently-tagged proteins are nonfunctional (as indicated by the lack of mutant complementation; see Fig. S4). Consequently, one should consider the ZicK/ZacK heteropolymer localization as observed here with a grain of salt. We suggest that the observed filaments are indicative of ZicK and ZacK heteropolymerization in the cell. (C) Electron micrographs of ultrathin sections of *Anabaena* WT and *Anabaena* cells co-expressing ZicK-eCFP and ZacK-GFP. Black arrows indicate electron-dense structures coinciding with the ZicK/ZacK heteropolymer observed in B. Figure C shows representative result from several independent trichomes investigated in a single experiment. Scale bars: 1.6 μm .

electron-dense filament-like structures in ultrathin sections using electron microscopy (Fig. 3C). Nonetheless, we could not identify similar filamentous structures in *Anabaena* WT electron micrographs. Thus, our results identify the general potential of ZicK and ZacK to form a heteropolymer *in vivo*, yet, the frequency and scale of the ZicK/ZacK heteropolymer in the wild-type remains an open question. To confirm that the localization of fluorophore-tagged ZicK and ZacK is not affected by the wild-type (WT) *zicK* or *zacK* alleles, we additionally localized both proteins individually or together in a $\Delta zicK\Delta zacK$ double mutant. These experiments revealed the same localization pattern as in *Anabaena* WT, suggesting that natively present ZicK or ZacK proteins do not affect the formation of ZicK-GFP, ZacK-GFP or the ZicK-eCFP/ZacK-GFP heteropolymer (Fig. S4B,C). The intracellular localization of the ZicK/ZacK heteropolymer in *Anabaena* indicates that the polymer is either anchored at the cell poles or specifically split during cell division, as ZicK/

ZacK filament-like structures were never observed to cross cell-cell borders and only traversed through not yet fully divided cells (Fig. 3B inlay and Fig. 3C). To further explore whether the ZicK/ZacK heteropolymer assembly is restricted to *Anabaena*, we proceeded to analyse ZicK and ZacK *in vivo* in an unrelated heterologous system using the *E. coli* split GFP assay [50]. Clearly, discernible filamentous-like structures (reminiscent of FilP-GFP [20]) could be detected upon co-expression of ZicK and ZacK C-terminally fused to the split GFP products (ZicK-NGFP and ZacK-CGFP; Fig. S5). This is in agreement with the lack of discernible structures upon expression of N-terminally GFP-fused ZicK and ZacK in *Anabaena*. Nonetheless, some indications for heteropolymerization were also present upon co-expression of NGFP-ZicK with ZacK-CGFP, which is in agreement with the BACTH results that indicated that both, N and C-terminal fusions of ZicK and ZacK, are potentially able to interact with each other (Fig. 2B). The different

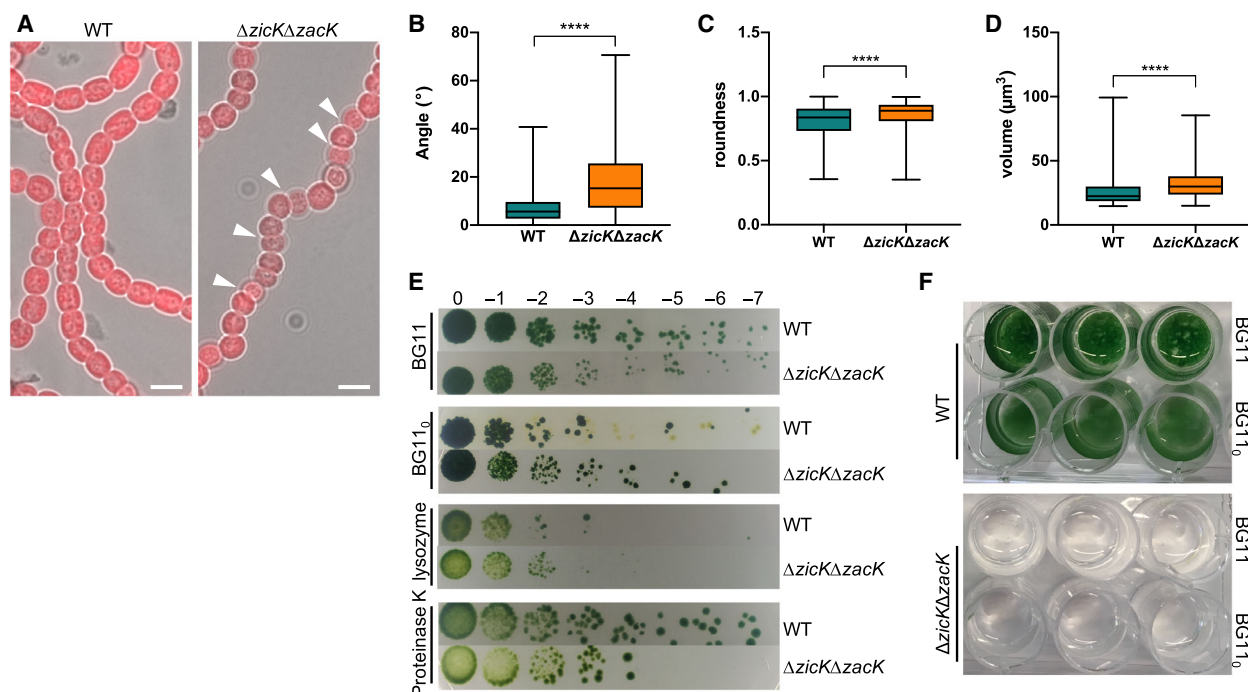


Fig. 4. Deletion of *zicK* and *zacK* alters trichome and cell shape as well as trichome viability. (A) Merged chlorophyll autofluorescence and bright-field micrographs of *Anabaena* WT and $\Delta zicK\Delta zacK$ mutant grown on BG11 plates. Note: only one fully segregated mutant was obtained in our study and figures here show representative micrographs of more than three independent experiments. White triangles indicate zigzagged trichome growth. Scale bars: 5 μm . (B) Measurement of the angle between neighbouring cells in *Anabaena* WT and the $\Delta zicK\Delta zacK$ mutant (*Anabaena* WT: $n = 388$; $\Delta zicK\Delta zacK$: $n = 447$; whiskers indicate minimal and maximal values for each group) (C) Cell roundness and (D) volume of *Anabaena* WT and $\Delta zicK\Delta zacK$ mutant measured with *IMAGEJ* imaging software. A perfect circle is defined as roundness of 1. Whiskers indicate minimal and maximal values for each group. Error bars indicate standard deviations. *Anabaena* WT: $n = 537$; $\Delta zicK\Delta zacK$: $n = 404$. Values indicated with asterisks are significantly different from the WT. **** $P < 0.0001$ (Student's *t*-test). (E) *Anabaena* WT and $\Delta zicK\Delta zacK$ mutant were spotted onto BG11, BG11₀ or BG11 plates supplemented with lysozyme or Proteinase K in triplicates of serial dilutions of factor 10 and grown until no further colonies arose in the highest dilution ($n = 2$). (F) *Anabaena* WT and $\Delta zicK\Delta zacK$ mutant were grown on BG11 plates, transferred to liquid BG11 and BG11₀ medium and incubated for 12 days at standard growth conditions without shaking.

heteropolymerization phenotype of ZicK/ZacK polymer in *E. coli* and *Anabaena* suggests that there are other so far unknown factors that modulate the specific ZicK/ZacK heteropolymerization phenotype, as highlighted in the following sections.

Deletion of *zicK* and *zacK* leads to defects in trichome and cell shape and *Anabaena* viability

In contrast to the obtained $\Delta zicK\Delta zacK$ double mutant, single $\Delta zicK$ or $\Delta zacK$ mutant strains could not be generated, suggesting that the presence (or absence) of ZicK or ZacK alone is lethal for *Anabaena*. Further investigating the $\Delta zicK\Delta zacK$ mutant phenotype revealed an altered trichome and cell shape phenotype and a reduced trichome viability (Fig. 4). Unlike the linear trichome growth pattern of the WT, the $\Delta zicK\Delta zacK$ mutant strain mostly grew as

zigzagged trichomes (Fig. 4A,B), a phenotype that could be rescued by heterologous expression of $P_{zicK}::zicK-zacK$ from pRL25C but not from $P_{zicK}::zicK-ecfp+zacK-gfp$ (Figs S4C and S6A). Additionally, $\Delta zicK\Delta zacK$ cells were significantly larger (WT: $27.42 \pm 14.75 \mu\text{m}^3$; $\Delta zicK\Delta zacK$: $32.52 \pm 12.54 \mu\text{m}^3$; $P < 0.0001$; Student's *t*-test) and significantly more round (defined as the mean of $4 \times \text{cell area} / (\pi \times \text{major_axis}^2)$; WT: 0.8063 ± 0.1317 ; $\Delta zicK\Delta zacK$: 0.8530 ± 0.1130 ; $P < 0.0001$; Student's *t*-test) in comparison with the WT (Fig. 4C,D), reminiscent of the $\Delta mreB$ mutant strain [38]. The round and swollen cell phenotypes of the $\Delta zicK\Delta zacK$ mutant strains are indicative of an impairment in cell wall integrity and/or defects in PG biogenesis as well as an elevated sensitivity to turgor pressure [51,52]. Consequently, we tested for an elevated sensitivity of the $\Delta zicK\Delta zacK$ mutant to cell wall damaging enzymes. This showed

that the $\Delta zicK\Delta zacK$ mutant is slightly more sensitive to Proteinase K treatment but was unaffected by lysozyme treatment and still retained the ability to grow diazotrophically (i.e., on BG11₀ plates) (Fig. 4E) and to form heterocysts (Fig. S6B). More importantly, however, we found that the $\Delta zicK\Delta zacK$ mutant lost the ability to grow in liquid culture (with and without agitation; Fig. 4F), hinting for an elevated sensitivity to fluid shear stress or turgor pressure. This defect could be complemented by heterologous expression of $P_{zicK}::zicK-zacK$ from pRL25C (Fig. S6C). We note, however, that we could not fully complement the mutant phenotype using our in trans complementation system as indicated by the decreased growth rate and seemingly smaller cell volumes (Fig. S6A,C), likely due to the variation in copy number of pRL25C [53].

ZicK and ZacK interact with proteins involved in cell shape and trichome integrity

Considering the impact of the deletion of *zicK* and *zacK* on cell and trichome shape and the assumed septal docking of the ZicK/ZacK heteropolymer, we next wanted to investigate whether both, ZicK and ZacK, physically interact with other proteins known to function in cell shape determination and cell–cell communication. Using the BACTH assay, we found that both, ZicK and ZacK, interacted with the divisome-associated septal protein SepI [49], the septal protein SepJ [54], the cell shape-determining protein MreB as well as an elongasome associated protein (ZipM; covered in more detail in subsequent study) and the *Anabaena* homolog to HmpF (here named HmpF_{Ana}), whose homologs were shown to be involved in motility in *Nostoc punctiforme* ATCC 29133 [55] and *Synechocystis* sp. PCC 6803 [42] (Fig. 5A). No interactions were found with FtsZ, FraC and FraD (Fig. S7). We attempted to further confirm our interaction results with affinity co-elution experiments but found that NiNTA-bound ZicK and ZacK purified from *E. coli* readily precipitated upon transfer from denaturing to native buffer conditions, precluding further co-elution studies. Additionally, we observed that nondenaturing conditions failed to purify overexpressed CCRPs from *E. coli*, confirming their inherent insoluble nature, a property known to eukaryotic IFs [56]. Instead, we surveyed for further interaction partners by anti-GFP co-immunoprecipitation experiments of *Anabaena* cells expressing ZicK-GFP and analysed coprecipitated proteins by LC-MS/MS analytics (all 27 identified possible interactors are listed in File S3). This analysis confirmed that ZicK and ZacK interact with each other *in vivo* and further strengthened the observed association

of ZicK with MreB (Fig. 5B). Furthermore, ZicK coprecipitated ParA (Fig. 5B), a Walker A-type ATPase, involved in chromosome and plasmid partitioning [57].

Deletion of *zicK* and *zacK* affects the localization of MreB and the chromosomes

As our BACTH analysis identified SepI and SepJ as interaction partners, and both proteins are involved in intercellular transport and cell–cell communication in *Anabaena* [49,58], we proceeded to test whether the $\Delta zicK\Delta zacK$ mutant is also affected in solute diffusion using fluorescence recovery after photobleaching (FRAP) experiments of calcein-stained $\Delta zicK\Delta zacK$ mutant. However, this analysis did not reveal any defect in cell–cell communication in the $\Delta zicK\Delta zacK$ mutant (Fig. S8A–C), and hence, ZicK and ZacK do not affect septal junction functionality. Additionally, electron microscopy of ultrathin sections of the $\Delta zicK\Delta zacK$ mutant did not show any discernible differences in the ultrastructure of the cells compared to cells of *Anabaena* WT (Fig. S8D). In accordance with a lack of interaction between FtsZ and ZicK/ZacK, FtsZ placement was unaffected in the $\Delta zicK\Delta zacK$ mutant as shown using anti-FtsZ immunofluorescence (Fig. S9A). Following the lead of ZicK/ZacK interaction partners, we next analysed the localization of MreB in the *Anabaena* WT and the $\Delta zicK\Delta zacK$ mutant using a functional $P_{petE}::gfp-mreB$ fusion [38]. In *Anabaena* WT, we predominantly observed GFP-MreB filaments throughout the cells without any directional preferences (96% or 202 of 211 counted cells) and rarely cell pole-localized foci (4% or 9 of 211 counted cells) (Fig. 6A). Even though GFP-MreB filaments were present in 40% (81 of 199 counted cells) of the $\Delta zicK\Delta zacK$ mutant cells expressing GFP-MreB (Fig. 6A inlay), we only detected those filaments in nonrounded cells that seemingly had a WT-like phenotype (Fig. 6A). In contrast, in rounded/swollen cells of zigzagged trichomes, GFP-MreB was mostly (60% or 118 of 199 counted cells) restricted to the cell poles (Fig. 6A). WT-like nonrounded cells accounted for about 24% of the $\Delta zicK\Delta zacK$ mutant cells expressing GFP-MreB (245 of 1040 cells counted), whereas rounded/swollen cells of zigzagged trichomes accounted for 76% of counted $\Delta zicK\Delta zacK$ mutant cells (795 of 1040 counted cells; note that not all cells counted for cell shape characteristics also contained GFP-MreB signals, thus explaining the discrepancies between the different counted cell numbers. This is likely due to the copy number variation of the pRL25C plasmid). To further investigate the potential

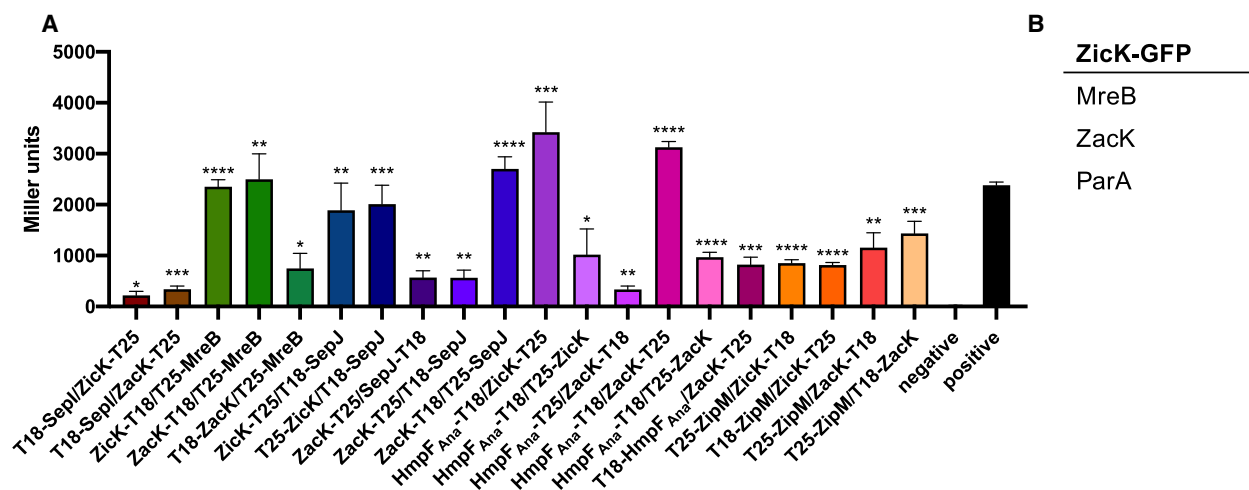


Fig. 5. ZicK and ZacK interact with a multitude of *Anabaena* proteins involved in cell shape and multicellularity. (A) BACTH assays of *Escherichia coli* cells co-expressing indicated T25 and T18 translational fusions of indicated pair-wise combinations of ZicK, ZacK, SepJ, MreB, SepJ, HmpF_{Ana} and ZipM. Only translational fusion combinations that resulted in a significant interaction between two analysed proteins are shown. All other combinations were negative for interaction. Note that we used full-length proteins for all our BACTH analysis, including SepJ, whose precise subcellular localization remains to be identified [49,97] but could be different in *E. coli* and *Anabaena* [49]. Quantitative values are given in Miller units, and the mean results from three independent colonies are presented. Negative control: T25-ZacK encoding plasmid cotransformed with empty pUT18C plasmid. Other negative controls using N-terminally T25-tagged proteins together with empty pUT18C plasmid resulted in equivalent values. Positive: Zip/Zip control. Error bars indicate standard deviations ($n = 3$). Values indicated with asterisks are significantly different from the negative control. * $P < 0.05$, ** $P < 0.005$, *** $P < 0.0005$, **** $P < 0.0001$ (Student's t -test). (B) Excerpt of the identified specific interactors of ZicK-GFP. The full list is listed in File S3.

effect of *zicK* and *zacK* deletion on MreB and hence elongasome function, we stained sites of active cell wall biosynthesis using a fluorescent vancomycin derivative (Van-FL; [59]). The staining pattern between the WT and the $\Delta zicK\Delta zacK$ mutant was indistinguishable but the fluorescence intensity levels were slightly decreased in the $\Delta zicK\Delta zacK$ mutant (Fig. S9B,C). Nonetheless, this is likely accounted for by the reduced growth rate of the $\Delta zicK\Delta zacK$ mutant (Fig. 4E and general observation on growth plates).

Considering the interaction of ZicK/ZacK with ParA, we further tested for a function of ZicK and ZacK in DNA placement and compared the DNA distribution in the WT and the $\Delta zicK\Delta zacK$ mutant as measured by distribution of 4',6-diamidino-2-phenylindol (DAPI) staining intensity (Fig. 6B,C). For that, we calculated the width of the DAPI focal area as the range of DAPI staining around the maximum intensity focus (± 10 grey intensity in arbitrary units). This revealed that the staining focal area size was significantly different among the WT and the $\Delta zicK\Delta zacK$ mutant. The DAPI signal observed in the $\Delta zicK\Delta zacK$ mutant appears more condensed, and indeed, the $\Delta zicK\Delta zacK$ mutant focal DAPI area was smaller than the WT (Fig. 6C). Unlike the WT, DAPI signals in the $\Delta zicK\Delta zacK$ mutant were also observed between two

neighbouring cells (Fig. 6B). Overall, our results may suggest the involvement of ZicK/ZacK in DNA distribution and segregation in dividing cells.

Discussion

Here, we provide evidence for the general capacity of two *Anabaena* CCRPs, which we termed ZicK and ZacK, to form polymers *in vitro* and *in vivo*. While the previously described prokaryotic filament-forming CCRPs formed homopolymers [17,19,20,60], ZicK and ZacK exclusively assembled into a heteropolymer *in vitro* and *in vivo*, thus revealing a new property of bacterial CCRPs. The inherent heteropolymerization tendency of ZicK and ZacK was confirmed in a heterologous and evolutionary distant *E. coli* system, which was previously used to investigate other known CCRPs such as Scc from *Leptospira biflexa* [61] or Crescentin [62]. Although heteropolymerization has previously been described for prokaryotic cytoskeletal proteins, none of those polymerization pairs both belonged to the group of CCRPs. BacA and BacB, members of the widely conserved class of bactofilins, both independently polymerize into filaments *in vitro*, colocalize *in vivo* in *C. crescentus* and interact directly with each other as indicated by co-

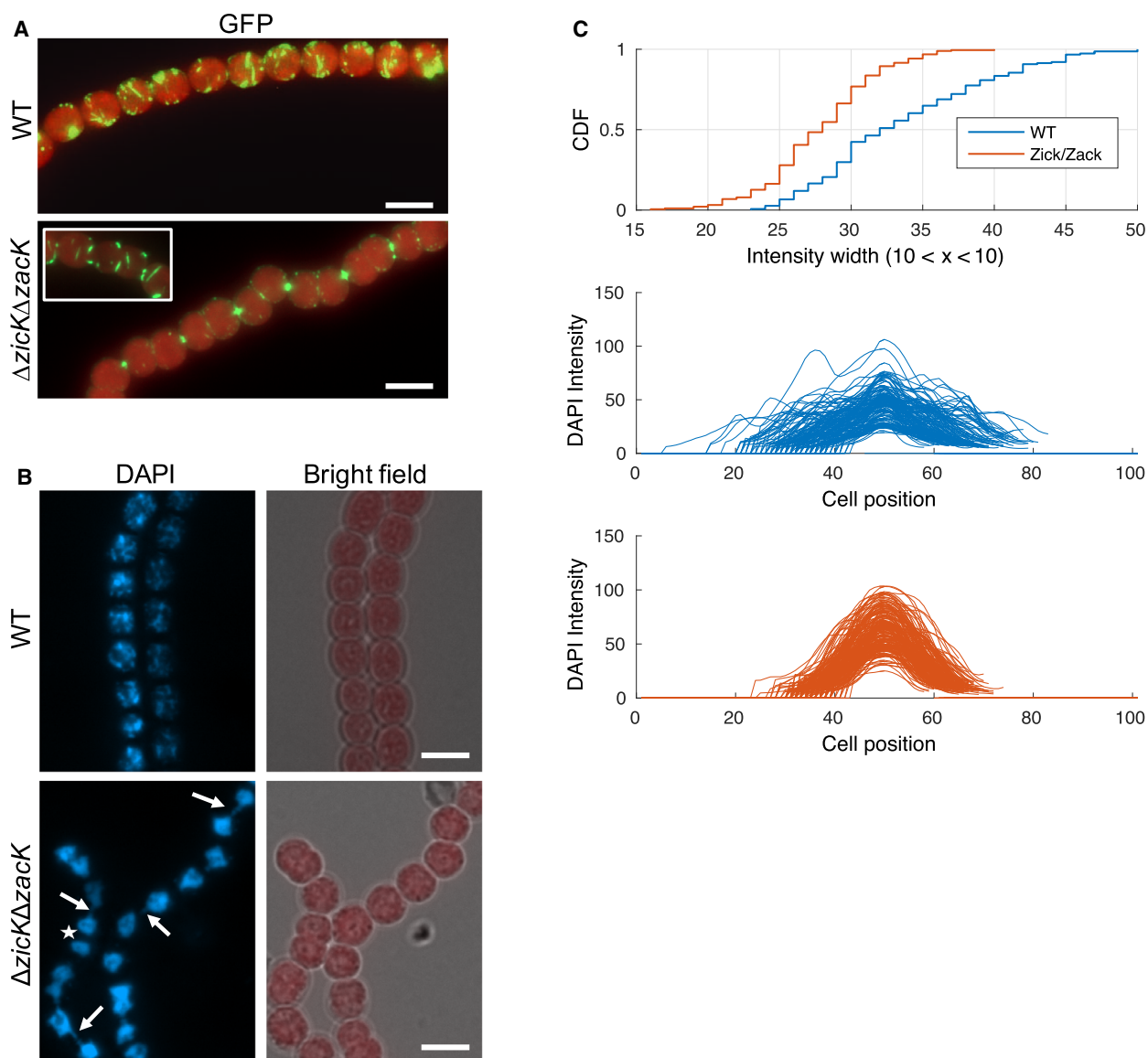


Fig. 6. Effect of *zicK* and *zacK* deletion on MreB localization and DNA distribution. (A) Merged GFP fluorescence and chlorophyll autofluorescence micrographs of *Anabaena* WT and $\Delta zicK\Delta zacK$ mutant expressing GFP-MreB from P_{petE} . Cells were grown on BG11 plates. Scale bars: 5 μ m. Inlay shows clear MreB filaments in cells displaying WT-like cell shapes of the $\Delta zicK\Delta zacK$ mutant. (B) DAPI fluorescence and merged bright-field and chlorophyll autofluorescence micrographs of *Anabaena* WT and $\Delta zicK\Delta zacK$ mutant on BG11 plates. White arrows indicate strings of DNA that seemingly traverse from one cell to the other. Notably, no such strings are observed in dividing cells (white star), suggesting that it is an effect that occurs after complete cell division. Although we note that high-resolution microscopy would be needed to fully resolve this observation. (A, B) Images presented are representatives from duplicate experiments. Scale bars: 5 μ m. (C) Plot profile showing a cumulative distribution function (CDF) of the DAPI signal intensities of pixels (grey value) along the long axis of *Anabaena* WT and $\Delta zicK\Delta zacK$ mutant cells ($n = 151$ for each strain) in arbitrary units (a.u.) and arranged to the respective peak maxima. The focal area size in the $\Delta zicK\Delta zacK$ mutant was smaller in comparison with the *Anabaena* WT ($P = 6.8 \times 10^{-117}$, using Wilcoxon test). Notably, the comparison of cell length among the strains reveals a similar result: the $\Delta zicK\Delta zacK$ mutant cell size was smaller in comparison to the *Anabaena* WT ($P = 7.2 \times 10^{-117}$, using Wilcoxon test). Consequently, we compared the area of the focal DAPI staining decided by the cell size among the strains. This, however, revealed that this ratio is not significantly different between the $\Delta zicK\Delta zacK$ mutant and the *Anabaena* WT.

immunoprecipitation analysis. Unlike CCRPs, whose self-interaction is based on the high degree of CC domains, in bactofilins, the DUF583 domain is

proposed to mediate protein polymerization [63]. Despite compelling evidence for co-assembly and shared functional properties, heteropolymerization of

BacA and BacB has not been studied *in vitro*. Another interesting pair of potential copolymerizing cytoskeletal proteins that both independently assemble into homopolymers but also co-align *in vivo* and affect each other's properties are Crescentin and the CtpS enzyme from *C. crescentus* [62]. However, again, the co-assembly *in vitro* is not reported in the literature.

Despite the numerous independently confirmed heteropolymerization properties of ZicK and ZacK, we note that the results from our *in vivo* experiments are based on artificial and heterologous expression of the two CCRPs and thus in itself could lead to artefacts. We hypothesize that the absence of a ZicK/ZacK heteropolymer in strains expressing ZicK-GFP or ZacK-GFP alone (with the WT *zicK* and *zacK* alleles still present) may be due to a dosage-dependent effect, where the presence of unequal concentration of ZicK or ZacK in the cell leads to protein aggregates. Our observation of ZicK-GFP or ZacK-GFP aggregates upon expression alone in the $\Delta zicK\Delta zacK$ mutant strain supports the dosage effect hypothesis. Also, in our *in vitro* polymerization assay, ZicK and ZacK only formed clear and distinct filament-like structures when both proteins are present in equal concentrations. Nonetheless, co-expression of ZicK-eCFP and ZacK-GFP could not complement the $\Delta zicK\Delta zacK$ mutant. Attempts to express both proteins fused to a fluorophore from the native promoter remained unsuccessful, possibly a result of the close genomic proximity. Furthermore, the genomic neighbourhood of *zicK* and *zacK* suggests that the ZicK/ZacK heteropolymer formation could be relying on cotranslational assembly (e.g., as observed for LuxA/LuxB [64]). Cotranslational assembly of natively present ZicK and ZacK would lead to an efficient binding of the two subunits such that the additional expression of one unit only in excess (i.e., ZicK-GFP or ZacK-GFP alone) would lead to the formation of aggregates. As such, it remains to be elucidated to what extent the ZicK/ZacK heteropolymer actually exists in *Anabaena* WT. Although we could not identify any protein filaments in our ultrathin sections from *Anabaena* WT, other studies have previously described filamentous strings and even longitudinal cell-spanning polymers in multicellular *Anabaena* and *Nostoc* strains [65,66]. Despite compelling evidence for the existence of a cyanobacterial Z-ring structure during cell division [48,67], no Z-ring ultrastructures have yet been identified, and consequently, the absence of longitudinal ZicK/ZacK filaments in ultrathin sections does not rule out that they exist but could also indicate that they could not be visualized yet.

Our results indicate that ZicK and ZacK are associated with the elongasome (through their interaction

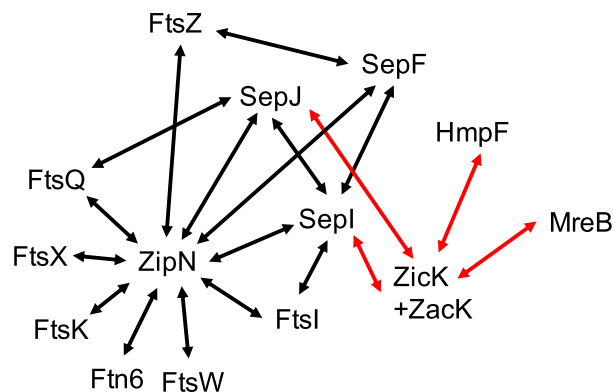


Fig. 7. Interaction network of known divisome, elongasome and septal proteins in *Anabaena*. A model for a partial divisome, elongasome and septal junction network in *Anabaena* as deduced from BACTH and co-IP analyses. Black arrows indicate interactions that have been previously described by [33,49,67]. Red arrows indicate interactions identified in the current analysis.

with MreB) and proteins in the septal cell wall (through the interaction with SepJ and SepI) and might affect cellular DNA placement (Fig. 7). A function of ZicK/ZacK in chromosome segregation would be in concert with the identified interaction of ZicK with ParA; this, however, remains to be elucidated as it could also be an indirect consequence of the swollen/rounded cell shape in the $\Delta zicK\Delta zacK$ mutant, similar to the indirect effect of *mreB* deletion of carboxysome alignment in *Synechococcus elongatus* PCC 7942 [68]. Nonetheless, so far, no chromosome partitioning system has yet been identified in multicellular cyanobacteria. In *Anabaena*, deletion of *mreB* did not affect chromosome segregation but induced a swollen cell phenotype [38], similar to the $\Delta zicK\Delta zacK$ mutant. Consequently, MreB and ZicK/ZacK likely share functional properties but are not exclusively involved in the same cellular processes. Swollen cell morphotypes were also described for *Anabaena* or *Synechocystis* mutants lacking penicillin-binding proteins (PBPs), which are enzymes that are directly involved in cell wall biogenesis through the modification of the PG layer [39]. This presumed link of ZicK/ZacK to the actin-like MreB cytoskeleton and the PG biogenesis apparatus is also indicated by the altered localization of GFP-MreB and the decreased PG staining intensity in the $\Delta zicK\Delta zacK$ mutant strain. Consequently, ZicK and ZacK might indirectly act to positively regulate PG biogenesis, although we cannot exclude that the reduced staining intensity in the $\Delta zicK\Delta zacK$ mutant simply reflects the slower growth rate of this strain. An interaction or involvement of prokaryotic filament-forming CCRPs with MreB and

PG synthesis was previously observed in other bacteria. Examples are the gliding motility in *Myxococcus xanthus*, where a multiprotein complex, including the filament-forming CCRP AglZ and MreB, was found to coordinate type A-motility [69]. Similarly, the curved morphotype of *C. crescentus* is induced by Crescentin, which functionally associates with MreB and likely modulates PG biogenesis by exuding local mechanical forces to the cell membrane [16,21]. Other aspects like a decreased cell envelope permeability of the $\Delta zicK\Delta zacK$ mutant are also conceivable, although we did not detect any cell wall defects in the $\Delta zicK\Delta zacK$ mutant. MreB and the elongasome are the main determinants of the PG exoskeleton, which provides the cell with structural integrity and resistance to turgor pressure [70]. The lack of liquid growth of the $\Delta zicK\Delta zacK$ mutant would also argue for a defect in the resistance to turgor pressure.

Together with the cell shape-determining protein MreB, ZicK and ZacK could possibly contribute to normal cell shape and relay trichome shape-stabilizing properties to neighbouring cells in the trichome by means of their association with the filament stabilizing protein SepJ (Fig. 7). As such, they are important for maintaining the linear *Anabaena* trichome phenotype. ZicK and ZacK polymers might constitute stabilizing platforms or scaffolds for other proteinaceous structures, similarly to the stabilizing function of the eukaryotic cytoskeleton for cell–cell contacts (i.e., desmosomes). Furthermore, ZicK shares *in silico* predicted structural similarities with the spectrin repeats of plectin, a well-described eukaryotic cytolinker protein. Plectin links the three eukaryotic cytoskeletal systems (actin filaments, microtubules and IFs), thereby contributing to the resistance to deformation of vertebrate cells [12]. They stabilize desmosomes and are hence directly involved in cell–cell contact integrity [71]. An analogous cytolinker function of ZicK could explain why ZacK alone did not form properly folded protein filaments on its own and suggests that ZacK requires ZicK as the linking protein for polymerization. As plectin not only stabilizes but also dynamically disassembles IF protein filaments (i.e., vimentin) in a concentration-dependent manner [72], this would further support a dosage-dependent effect of ZicK and ZacK for heteropolymerization.

The ubiquity of ZicK and ZacK in heterocystous cyanobacteria that form linear trichomes (Fig. 1C, File S2) indicates that the presence of ZicK and ZacK contributes to the maintenance of a linear trichome shape. The $\Delta zicK\Delta zacK$ mutant had a zigzagged phenotype and was unable to grow in liquid culture. We hypothesize that the loss of linear trichome shape led to an

increase in accessible surface for the acting mechanical forces in liquid [73], including fluid shear stress [74], ultimately resulting in forces that cannot be endured by the abnormal mutant trichomes. Nonetheless, the absence of ZicK and/or ZacK in several heterocystous cyanobacteria species, including the fern-symbiont *N. azollae* and ramified cyanobacteria, may suggest that these species are less sensitive to mechanical stress (i.e., due to their interaction with the host tissues or complex filament formation), and hints for the presence of additional, yet unknown, mechanisms for the determination of filament shape.

The key hallmarks of permanent bacterial multicellularity are morphological differentiation and a well-defined and reproducible shape, termed patterned multicellularity [75]. In sporulating actinomycetes, this is exemplified by the highly reproducible cell division, cell proliferation and cell differentiation pattern [76]. In filamentous cyanobacteria, the reproducible linear trichomes are considered a major contributor to the cyanobacterial patterned multicellularity [75], manifesting a selective advantage to biotic and abiotic environmental factors [77,78]. Our results indicate that ZicK and ZacK serve as regulators of the typical linear *Anabaena* trichome and as such as regulators of *Anabaena* patterned multicellularity. The evolution of patterned multicellularity is considered an important step towards a sustainable division of labour and the development of cell differentiation [75]. Our study provides initial evidence for a role of two heteropolymer-forming CCRPs in the evolution and maintenance of cyanobacterial multicellular forms.

Materials and methods

Bacterial strains and growth conditions

Anabaena sp. PCC 7120 was obtained from the Pasteur Culture Collection (PCC) of cyanobacteria (France). Cells were grown photoautotrophically in BG11 or without combined nitrogen (BG11₀) at constant light with a light intensity of 30 $\mu\text{mol}\cdot\text{m}^{-2}\cdot\text{s}^{-1}$ in liquid culture or on agar plates (1.5% w/v agar). When appropriate, 5 $\mu\text{g}\cdot\text{mL}^{-1}$ spectinomycin (Sp), 5 $\mu\text{g}\cdot\text{mL}^{-1}$ streptomycin (Sm) or 30 $\mu\text{g}\cdot\text{mL}^{-1}$ neomycin (Nm) was added to strains carrying respective plasmids or chromosomal insertions. In some cases, basal copper-regulated *petE*-driven expression of gene candidates in *Anabaena* cells was lethal or growth inhibiting, therefore these strains were grown in BG11 without copper and protein expression was later induced by the addition of CuSO_4 at indicated concentrations to the culture. *E. coli* strains DH5 α , DH5 α MCR, XL1-blue and HB101 were used for cloning and conjugation by triparental mating. BTH101

was used for BACTH system, and BL21 (DE3) was used for expression of His₆-tagged proteins in *E. coli*. All *E. coli* strains were grown in LB medium containing the appropriate antibiotics at standard concentrations. Tables S1–S4 list all used bacterial strains, plasmids and oligonucleotides.

Prediction of coiled-coil-rich proteins

Genome sequence of *Anabaena* (GCA_000009705.1) was analysed by the COILS algorithm [79] as previously described [20]. The algorithm was run with a window width of 21, and the cut-off for amino acids in coiled-coil conformation was set to ≥ 80 amino acid residues. The resulting set of protein candidates was further manually examined with online available bioinformatic tools, including NCBI conserved domain search [80], NCBI BLAST [81], TMHMM [82] and I-TASSER [83]. Protein candidates exhibiting BLAST hits involved in cytoskeletal processes or similar domain architectures as known IF and IF-like proteins like Crescentin, FilP, vimentin, desmin or keratin were selected, and enzymatic proteins as well as proteins predicted to be involved in other cellular processes were excluded.

Distribution of homologs in cyanobacteria

Homologs to the *Anabaena* proteins were extracted from precalculated cyanobacterial protein families [42]. Conserved syntenic blocks (i.e., gene order) were identified using CSBFinder-S [84].

RNA isolation and cDNA synthesis

RNA from *Anabaena* WT was isolated using the Direct-zol™ RNA MiniPrep Kit (Zymo Research, Freiburg, Germany) according to the manufacturer's instructions. RNA was isolated in technical triplicates from 10 mL cultures. Isolated RNA was treated with DNA-free™ Kit (2 units rDNAs/reaction; Thermo Fischer Scientific, Dreieich, Germany), and 200 ng RNA was reverse transcribed using the qScript™ cDNA Synthesis Kit (Quanta Biosciences, Beverly, MA, USA). RT-PCR of cDNA samples for *rnpB*, *zicK*, *zacK* and *zicK+zacK* was performed using primer pairs #1/#2, #3/#4, #5/#6 and #3/#8, respectively.

Transformation

Anabaena was transformed by triparental mating as previously described [85]. Briefly, 100 μ L of overnight cultures of DH5 α carrying the conjugal plasmid pRL443 and DH5 α MCR carrying the cargo plasmid and the helper plasmid pRL623, encoding for three methylases, were mixed with 200 μ L *Anabaena* culture (for transformation into the $\Delta zicK\Delta zacK$ mutant, cells were scraped from the plate and resuspended in 200 μ L BG11). This mixture was directly

applied onto sterilized nitrocellulose membranes (Amersham Protran 0.45 NC, Cytiva Europe, Freiburg, Germany) placed on top of BG11 plates supplemented with 5% (v/v) LB medium. Cells were incubated in the dark at 30 °C for 6–8 h with subsequent transfer of the membranes to BG11 plates, and plates were placed under standard growth conditions. After 24 h, membranes were transferred to BG11 plates supplemented with appropriate antibiotics.

Plasmid construction

Ectopic expression of *Anabaena* protein candidates was achieved from a self-replicating plasmid (pRL25C [86]) under the control of the copper-inducible *petE* promoter (P_{petE}) or the native promoter (predicted by BPROM [47]) of the respective gene. All constructs were verified by Sanger sequencing (Eurofins Genomics, Ebersberg, Germany). Plasmids were created using standard restriction enzyme-based techniques or Gibson assembly. Information about precise plasmid construction strategies is available from the authors upon request.

Anabaena mutant strain construction

The $\Delta zicK\Delta zacK$ mutant strain was generated using the pRL278-based double homologous recombination system employing the conditionally lethal *sacB* gene [87]. For this, 1500 bp upstream and downstream of *zicK-zacK* was generated by PCR from *Anabaena* gDNA. Upstream region of *zicK* was amplified using primers #97/#98, and downstream region of *zacK* was amplified using primers #99/#100. The respective upstream and downstream homology regions flanking the CS.3 cassette (amplified with primer #95/#96 from pCSEL24) were then inserted into PCR-amplified pRL278 (using primer #93/#94) by Gibson assembly, yielding pTHS166. *Anabaena* transformed with pTHS166 plasmids was subjected to several rounds of restreaking on new plates (about 5–8 rounds). To test for fully segregated clones, colony PCRs were performed. For this, *Anabaena* cells were resuspended in 10 μ L sterile H₂O of which 1 μ L was used for standard PCR with internal *zicK* and *zacK* gene primers #3/#6. Correct placement of the CS.3 cassette was then further confirmed using CS.3 cassette primers with binding sites outside of the 5' and 3' flanks used for homologous recombination (primers #95/#102 and #101/#96).

Fluorescence microscopy

Bacterial strains grown in liquid culture were either directly applied to a microscope slide or previously immobilized on a 2% (w/v) low-melting agarose in PBS (10 mM Na₂HPO₄, 140 mM NaCl, 2.7 mM KCl, 1.8 mM KH₂PO₄, pH 7.4) agarose pad and air-dried before microscopic analysis.

Epifluorescence was done using an Axio Imager.M2 light microscope (Carl Zeiss, Oberkochen, Germany) equipped with Plan-Apochromat 63x/1.40 Oil M27 objective and the AxioCam MR R3 imaging device (Carl Zeiss). GFP, Alexa Fluor 488 and BODIPY™ FL Vancomycin (Van-FL) fluorescence was visualized using filter set 38 [Carl Zeiss; excitation: 470/40 nm band-pass (BP) filter; emission: 525/50 nm BP]. Chlorophyll autofluorescence was recorded using filter set 15 (Carl Zeiss; excitation: 546/12 nm BP; emission: 590 nm long pass). When applicable, cells were previously incubated in the dark at RT for about 5 min with 10 µg·mL⁻¹ DAPI (final concentration) to stain intracellular DNA. For visualization of DAPI fluorescence filter set 49 (Carl Zeiss; excitation: G 365 nm; emission: 455/50 nm) was employed. For confocal laser scanning microscopy, the LSM 880 Axio Imager 2 equipped with a C-Apochromat 63x/1.2 W Korr M27 objective and an Airyscan detector (Carl Zeiss) was used and visualization of GFP, eCFP and chlorophyll autofluorescence was done using Zen black smart setup settings.

Transmission electron microscopy

For ultrastructure analysis, *Anabaena* trichomes were fixed with 2.5% (v/v) glutaraldehyde, immobilized in 2% (w/v) agarose, treated with 2% (v/v) potassium permanganate and dehydrated through a graded ethanol series [88]. The fixed cells were infiltrated by ethanol : EPON (2 : 1 to 1 : 2 ratio) and embedded in pure EPON. Ultrathin sections were prepared with a Leica UC6i Ultramicrotome, transferred to formvar-coated copper grids (Science Services GmbH München) and poststained with uranyl acetate and lead citrate [89]. Micrographs were recorded at a Philips Tecnai10 electron microscope (FEI, Hillsboro, OR, USA) at 80 kV.

Calcein labelling and fluorescence recovery after photobleaching experiments

For FRAP experiments, *Anabaena* WT and $\Delta zicK\Delta zacK$ mutant strain were grown on BG11 plates, resuspended in BG11 liquid media and washed three times in 1 mL BG11 (3000 g, 5 min). Cells were then resuspended in 0.5 mL BG11 and incubated with 10 µL calcein-AM (Cayman Chemical, Ann Arbor, MI, USA; 1 mg·mL⁻¹ in DMSO) for 1 h at 30 °C in the dark. To remove excess staining solution, the cells were washed four times with 1 mL BG11. Subsequently, the cells were spotted on BG11 agar for visualization by confocal laser scanning microscopy (Leica TCS SP5; HCX PL APO 63x 1.40-0.60 OIL CS). Calcein was excited at 488 nm and fluorescence emission monitored in the range from 500 to 530 nm with a maximally opened pinhole (600 µm). FRAP experiments were carried out by an automated routine as previously

described [58]. After recording an initial image, selected cells were bleached by increasing the laser intensity by a factor of 5 for two subsequent scans and the fluorescence recovery followed in 0.5-s intervals for 30 s was recorded using the Leica LAS X software. Exchange coefficients (E) were then calculated as previously described [58,90].

BODIPY™ FL vancomycin (Van-FL) staining

Van-FL staining of strains grown on BG11 plates was essentially performed as described previously [91,92]. Briefly, cells were resuspended in BG11 medium, washed once in BG11 by centrifugation (6500 g, 4 min, RT) and incubated with 5 µg·mL⁻¹ Van-FL (dissolved in methanol; Thermo Fischer Scientific). Cells were incubated in the dark for 1 h at 30 °C, washed three times with BG11 and immobilized on an agarose pad. Van-FL fluorescence signals were then visualized using epifluorescence microscopy with an excitation time of 130 ms. Arithmetic mean fluorescence intensities were recorded from the septa between two cells with a measured area of 3.52 µm² using the histogram option of the ZEN BLUE 2.3 software (Carl Zeiss).

Alcian blue staining

Anabaena WT and $\Delta zicK\Delta zacK$ cells were grown on BG11₀ plates, resuspended in BG11₀ liquid medium and stained with 0.05% (w/v) alcian blue (final concentration). Polysaccharide staining of cells immobilized on an agarose pad was observed with an AxioCam ERc 5s colour camera (Carl Zeiss).

Data analysis

Cell volume and roundness were determined using the imaging software IMAGEJ [93], and a perfect circle is defined to have a roundness of 1. Cell volume was calculated based on the assumption of an elliptic cell shape of *Anabaena* cells using the Major Axis and Minor Axis values given by IMAGEJ and the formula for the volume of an ellipsoid

$$\left(V = \frac{4}{3}\pi abc \right) = V = \frac{4}{3}\pi \left(\left(\frac{\text{Major Axis}}{2} \right)^2 \frac{\text{Minor Axis}}{2} \right).$$

Angles between neighbouring cells were determined from chlorophyll autofluorescence micrographs from individual *Anabaena* trichomes in IMAGEJ. For this, the trichomes were separated from the background using the 'set autothreshold' command. The adjustable Watershed plug-in was used to separate individual cells in one trichome (tolerance = 1). After selecting cells with the analyse particle command (size = 200–2000 pixel; circularity = 0.20–1.00), the centre of each cell was determined as XY coordinates using the centroid measurement setting. The angles between three of

these points, representing the angle change in the trichome at each cell, were then calculated using basic algebra in Microsoft excel.

Distribution of DAPI fluorescence signal intensity was analysed in IMAGEJ with the Plot Profile option along the long axis of 151 single cells with the rectangle tool. The resulting grey values were arranged according to the maximum intensity focus, and the width of the DAPI focal area was calculated as the range of DAPI staining around the maximum (± 10 grey value in arbitrary units). Statistical tests were performed with MATLAB[®] (MathWorks; Natick, MA, USA) or GRAPHPAD PRISM v.8 (GraphPad Software, San Diego, CA, USA).

Bacterial two-hybrid and beta-galactosidase assays

Chemically competent *E. coli* BTH101 cells were cotransformed with 5 ng of plasmids carrying the respective T18 and T25 translational fusion constructs, plated onto LB plates supplemented with 200 $\mu\text{g}\cdot\text{mL}^{-1}$ X-gal, 0.5 mM IPTG, Amp, Km and grown at 30 °C for 24–36 h. Interactions were quantified by beta-galactosidase assays from three independent colonies. For this aim, cultures were grown for 2 days at 20 °C in LB Amp, Km, 0.5 mM IPTG and beta-galactosidase activity was recorded as described in the manufacturer's instructions (Euromedex, Souffelweyersheim, France; BACTH System Kit Bacterial Adenylate Cyclase Two-Hybrid System Kit) in a 96-well plate format as previously described [94].

GFP-fragment reassembly assay

Chemically competent *E. coli* BL21 (DE3) were cotransformed with indicated plasmid combinations, plated on LB Amp, Km and grown overnight at 37 °C. Liquid overnight cultures of single colonies of the respective plasmid-bearing *E. coli* strains were then diluted 1 : 40 in the same medium the following day. Cells were grown for 2 h at 37 °C, briefly acclimated to 20 °C for 10 min, and protein expression was induced with 0.05 mM IPTG and 0.2% (w/v) L-arabinose. Pictures of induced cultures grown at 20 °C were taken 48 h after induction.

Co-immunoprecipitation

About 20–30 mL of the respective *Anabaena* cultures was pelleted by centrifugation (4800 g, 10 min, RT), cells were washed twice by centrifugation (4800 g, 10 min, RT) with 40 mL PBS and then resuspended in 1 mL lysis buffer [PBS-N: PBS with 1% (v/v) NP-40] supplemented with protease inhibitor cocktail (PIC; cOmplete[™], EDTA-free Protease Inhibitor Cocktail; Sigma-Aldrich, Steinheim, Germany). Cells were lysed using the VK05 lysis kit (Bertin

Instruments, Frankfurt am Main, Germany) in a Precellys[®] 24 homogenizer (3 strokes for 30 s at 6500 r.p.m.), and cell debris was pelleted by centrifugation (30 min, 21 100 g, 4 °C). 50 μL μMACS anti-GFP MicroBeads (Miltenyi Biotec, Bergisch Gladbach, Germany) were added to the resulting cell-free supernatant and incubated for 1 h at 4 °C with mild rotation. Subsequently, the sample was loaded onto $\mu\text{Columns}$ (Miltenyi Biotec), washed two times with 1 mL lysis buffer and eluted in 50 μL Elution Buffer [50 mM Tris/HCl pH 6.8, 50 mM DTT, 1% (w/v) SDS, 1 mM EDTA, 0.005% (w/v) bromophenol blue, 10% (v/v) glycerol; Miltenyi Biotec]. Samples were stored at -80 °C until further use.

Mass spectrometry

Mass spectrometry of coprecipitated proteins was performed as previously described [49].

Immunofluorescence

Immunolocalization of FtsZ in *Anabaena* WT and $\Delta\text{zicK}\Delta\text{zacK}$ mutant was essentially performed as previously described [33]. For this, strains were scraped off from growth plates (BG11 and BG11₀ plates), resuspended in a small volume of distilled water and air-dried on Polysine[®] adhesion slides (Menzel) at RT followed by fixation and permeabilization with 70% ethanol for 30 min at -20 °C. Cells were allowed to air dry for 30 min at RT and then washed two times with PBST [PBS supplemented with 0.1% (v/v) Tween-20] for 2 min. Unspecific binding sites were blocked for 30 min at RT with blocking buffer (1 \times Roti[®]-ImmunoBlock in PBST; Carl Roth, Karlsruhe, Germany), and afterwards, rabbit anti-FtsZ (Agriseria; raised against *Anabaena* FtsZ; 1 : 150 diluted) antibody in blocking buffer was added to the cells and incubated for 1.5 h at RT in a self-made humidity chamber followed by five washing steps with PBST. 7.5 $\mu\text{g}\cdot\text{mL}^{-1}$ (final concentration) Alexa Fluor 488-conjugated goat anti-rabbit IgG (H+L) secondary antibody (Thermo Fischer Scientific) in blocking buffer was added to the cells and incubated for 1 h at RT in the dark in a self-made humidity chamber. Subsequently, cells were washed five times with PBST, air-dried and mounted with ProLong[™] Diamond Antifade Mountant (Thermo Fischer Scientific) overnight at 4 °C. Immunolocalization of FtsZ was then analysed by epifluorescence microscopy.

Spot assays

For spot assays, *Anabaena* WT and $\Delta\text{zicK}\Delta\text{zacK}$ mutant strain was grown on BG11 growth plates, resuspended in BG11 liquid medium and adjusted to an OD₇₅₀ of 0.4. Cells were then spotted in triplicates of 5 μL onto the respective

growth plates containing either no additives (BG11 or BG11₀), 50 µg·mL⁻¹ proteinase K or 100 µg·mL⁻¹ lysozyme in serial 1/10 dilutions and incubated under standard growth conditions until no further colonies arose in the highest dilution.

Protein purification and *in vitro* filamentation assays

For protein purification, *E. coli* BL21 (DE3) cells carrying His-tagged protein candidates were grown in overnight cultures at 37 °C and 250 r.p.m. The next day, overnight cultures were diluted 1 : 40 in the same medium and grown at 37 °C until they reached an OD₆₀₀ of 0.5–0.6. Protein expression was induced with 0.5 mM IPTG for 3–4 h at 37 °C and 250 r.p.m. Afterwards, cell suspensions of 50 mL aliquots were harvested by centrifugation, washed once in PBS and stored at –80 °C until further use. For *in vitro* filamentation assays, cell pellets were resuspended in urea lysis buffer (ULB: 50 mM NaH₂PO₄, 300 mM NaCl, 25 mM imidazole, 6 M urea; pH 8.0) and lysed in a Precellys[®] 24 homogenizer (3× 6500 r.p.m. for 30 s) using the 2 mL microorganism lysis kit (VK01; Bertin) or self-packed Precellys tubes with 0.1-mm glass beads. The resulting cell debris was pelleted by centrifugation at 21 000 *g* (10 min, 4 °C), and the supernatant was incubated with 1 mL His-Pur[™] Ni-NTA resin (Thermo Fischer Scientific) for 1 h at 4 °C in an overhead rotator. The resin was washed five times with 4× resin-bed volumes ULB and eluted in urea elution buffer (UEB: ULB supplemented with 225 mM imidazole). Total protein concentration was measured using the Qubit[®] 3.0 Fluorometer (Thermo Fischer Scientific). Filament formation of purified proteins was induced by overnight dialysis against polymerization buffer (PLB: 50 mM PIPES, 100 mM KCl, pH 7.0; HLB: 25 mM HEPES, 150 mM NaCl, pH 7.4; or 25 mM HEPES pH 7.5) at 20 °C and 180 r.p.m. with three bath changes using a Slide-A-Lyzer[™] MINI Dialysis Device (10K MWCO, 0.5 mL or 2 mL; Thermo Fischer Scientific). Purified proteins were stained with an excess of NHS-fluorescein (dissolved in DMSO; Thermo Fischer Scientific), and *in vitro* filamentation was analysed by epifluorescence microscopy. The NHS-fluorescein dye was previously successfully used to visualize *in vitro* FtsZ and CCRP protein filaments [42,95]. And we note that the His₆-tag did not impact the *in vitro* polymerization properties of the CCRP FilP [25], confirming the applicability of our approach.

Acknowledgements

We thank Myriam Barz, Katrin Schumann, Lisa-Marie Philipp, Lisa Stuckenschneider and Claudia Menzel for their assistance in the experimental work, Andreas Tholey for help with the mass spectrometry analysis, Jan Michels for support with fluorescence microscopy and Fenna Stücker for creative support

with the graphical abstract. FRAP experiments were performed at the Facility for Imaging by Light Microscopy (FILM) at Imperial College London. This study was supported by the German science foundation (DFG) (Grant No. STU513/2-1) and a Fondecyt Grant (Grant No. 11170842), both awarded to KS. IM was supported by German science foundation (DFG) (Grant SFB766). DJN was supported by the BBSRC as part of the joint NSF Ideas Lab grant on ‘Nitrogen: improving on nature’ (Grant No. BB/L011506/1). Open access funding enabled and organized by Projekt DEAL.

Conflict of interest

The authors declare no conflict of interest.

Author contributions

BLS and KS designed the study. BLS established and performed the experimental work with contributions from MLT and JW. CW and TD performed comparative genomics analysis. DJN performed FRAP assays, and IM carried out ultrastructure analyses. AOH analysed protein samples by mass spectrometry. BLS, TD and KS drafted the manuscript with contributions from all co-authors.

Peer Review

The peer review history for this article is available at <https://publons.com/publon/10.1111/febs.15630>.

Data accessibility

All data generated or analysed during this study are included in this published article (and its Supporting Information).

References

- 1 Wagstaff J & Löwe J (2018) Prokaryotic cytoskeletons: protein filaments organizing small cells. *Nat Rev Microbiol* **16**, 187–201.
- 2 de Boer P, Crossley R & Rothfield L (1992) The essential bacterial cell-division protein FtsZ is a GTPase. *Nature* **359**, 254–256.
- 3 Nogales E, Downing KH, Amos LA & Löwe J (1998) Tubulin and FtsZ form a distinct family of GTPases. *Nat Struct Biol* **5**, 451–458.
- 4 den Blaauwen T, Hamoen LW & Levin PA (2017) The divisome at 25: the road ahead. *Curr Opin Microbiol* **36**, 85–94.

- 5 Bi E & Lutkenhaus J (1991) FtsZ ring structure associated with division in *Escherichia coli*. *Nature* **354**, 161–164.
- 6 Jones LJF, Carballido-López R & Errington J (2001) Control of cell shape in bacteria: helical, actin-like filaments in *Bacillus subtilis*. *Cell* **104**, 913–922.
- 7 van den Ent F, Amos LA & Löwe J (2001) Prokaryotic origin of the actin cytoskeleton. *Nature* **413**, 39–44.
- 8 Errington J & Wu LJ (2017) Cell Cycle Machinery in *Bacillus subtilis*. pp. 67–101. Springer, Cham.
- 9 Dagan T, Roettger M, Stucken K, Landan G, Koch R, Major P, Gould SB, Goremykin VV, Rippka R, De Marsac NT *et al.* (2013) Genomes of stigonematalean cyanobacteria (subsection V) and the evolution of oxygenic photosynthesis from prokaryotes to plastids. *Genome Biol Evol* **5**, 31–44.
- 10 Chen C, MacCready JS, Ducat DC & Osteryoung KW (2018) The molecular machinery of chloroplast division. *Plant Physiol* **176**, 138–151.
- 11 Schlieper D, Oliva MA, Andreu JM & Lowe J (2005) Structure of bacterial tubulin BtubA/B: evidence for horizontal gene transfer. *Proc Natl Acad Sci USA* **102**, 9170–9175.
- 12 Alberts B, Johnson A, Lewis J, Morgan D, Raff M, Roberts K & Walter P (2014) Molecular Biology of the Cell, 6th edn. Garland Science, New York, NY.
- 13 Fuchs E & Weber K (1994) Intermediate filaments: structure, dynamics, function and disease. *Annu Rev Biochem* **63**, 345–382.
- 14 Mason JM & Arndt KM (2004) Coiled coil domains: stability, specificity, and biological implications. *ChemBioChem* **5**, 170–176.
- 15 Herrmann H & Aebi U (2000) Intermediate filaments and their associates: multi-talented structural elements specifying cytoarchitecture and cytodynamics. *Curr Opin Cell Biol* **12**, 79–90.
- 16 Lin L & Thanbichler M (2013) Nucleotide-independent cytoskeletal scaffolds in bacteria. *Cytoskeleton* **70**, 409–423.
- 17 Ausmees N, Kuhn JR & Jacobs-Wagner C (2003) The bacterial cytoskeleton: an intermediate filament-like function in cell shape. *Cell* **115**, 705–713.
- 18 Holmes NA, Walshaw J, Leggett RM, Thibessard A, Dalton KA, Gillespie MD, Hemmings AM, Gust B & Kelemen GH (2013) Coiled-coil protein Scy is a key component of a multiprotein assembly controlling polarized growth in *Streptomyces*. *Proc Natl Acad Sci USA* **110**, E397–E406.
- 19 Specht M, Schätzle S, Graumann PL & Waidner B (2011) *Helicobacter pylori* possesses four coiled-coil-rich proteins that form extended filamentous structures and control cell shape and motility. *J Bacteriol* **193**, 4523–4530.
- 20 Bagchi S, Tomenius H, Belova LM & Ausmees N (2008) Intermediate filament-like proteins in bacteria and a cytoskeletal function in *Streptomyces*. *Mol Microbiol* **70**, 1037–1050.
- 21 Charbon G, Cabeen MT & Jacobs-Wagner C (2009) Bacterial intermediate filaments: In vivo assembly, organization, and dynamics of crescentin. *Genes Dev* **23**, 1131–1144.
- 22 Wickstead B & Gull K (2011) The evolution of the cytoskeleton. *J Cell Biol* **194**, 513–525.
- 23 Letek M, Ordóñez E, Vaquera J, Margolin W, Flärdh K, Mateos LM & Gil JA (2008) DivIVA is required for polar growth in the MreB-lacking rod-shaped actinomycete *Corynebacterium glutamicum*. *J Bacteriol* **190**, 3283–3292.
- 24 Surovtsev IV & Jacobs-Wagner C (2018) Subcellular organization: a critical feature of bacterial cell replication. *Cell* **172**, 1271–1293.
- 25 Javadi A, Söderholm N, Olofsson A, Flärdh K & Sandblad L (2019) Assembly mechanisms of the bacterial cytoskeletal protein FilP. *Life Sci Alliance* **2**, e201800290.
- 26 Fröjd MJ & Flärdh K (2019) Apical assemblies of intermediate filament-like protein FilP are highly dynamic and affect polar growth determinant DivIVA in *Streptomyces venezuelae*. *Mol Microbiol* **112**, 47–61.
- 27 Rippka R, Stanier RY, Deruelles J, Herdman M & Waterbury JB (1979) Generic assignments, strain histories and properties of pure cultures of cyanobacteria. *Microbiology* **111**, 1–61.
- 28 Corrales-Guerrero L, Mariscal V, Flores E & Herrero A (2013) Functional dissection and evidence for intercellular transfer of the heterocyst-differentiation PatS morphogen. *Mol Microbiol* **88**, 1093–1105.
- 29 Flores E, Herrero A, Forchhammer K & Maldener I (2016) Septal junctions in filamentous heterocyst-forming cyanobacteria. *Trends Microbiol* **24**, 79–82.
- 30 Herrero A, Stavans J & Flores E (2016) The multicellular nature of filamentous heterocyst-forming cyanobacteria. *FEMS Microbiol Rev* **40**, 831–854.
- 31 Weiss GL, Kieninger A-K, Maldener I, Forchhammer K & Pilhofer M (2019) Structure and function of a bacterial gap junction analog. *Cell* **178**, 374–384.e15.
- 32 Wilk L, Strauss M, Rudolf M, Nicolaisen K, Flores E, Kühlbrandt W & Schleiff E (2011) Outer membrane continuity and septosome formation between vegetative cells in the filaments of *Anabaena* sp. PCC 7120. *Cell Microbiol* **13**, 1744–1754.
- 33 Ramos-León F, Mariscal V, Frías JE, Flores E & Herrero A (2015) Divisome-dependent subcellular localization of cell-cell joining protein SepJ in the filamentous cyanobacterium *Anabaena*. *Mol Microbiol* **96**, 566–580.
- 34 Choi Y, Kim J, Yoon H-J, Jin KS, Ryu S & Lee HH (2018) Structural insights into the FtsQ/FtsB/FtsL complex, a key component of the divisome. *Sci Rep* **8**, 18061.

- 35 Zhang C-CC, Hugenin S, Friry A, Huguenin S & Friry A (1995) Analysis of genes encoding the cell division protein FtsZ and a glutathione synthetase homologue in the cyanobacterium *Anabaena* sp. PCC 7120. *Res Microbiol* **146**, 445–455.
- 36 Sakr S, Jeanjean R, Zhang C-C & Arcondeguy T (2006) Inhibition of cell division suppresses heterocyst development in *Anabaena* sp. strain PCC 7120. *J Bacteriol* **188**, 1396–1404.
- 37 Klint J, Rasmussen U & Bergman B (2007) FtsZ may have dual roles in the filamentous cyanobacterium *Nostoc/Anabaena* sp. strain PCC 7120. *J Plant Physiol* **164**, 11–18.
- 38 Hu B, Yang G, Zhao W, Zhang Y & Zhao J (2007) MreB is important for cell shape but not for chromosome segregation of the filamentous cyanobacterium *Anabaena* sp. PCC 7120. *Mol Microbiol* **63**, 1640–1652.
- 39 Burnat M, Schleiff E & Flores E (2014) Cell envelope components influencing filament length in the heterocyst-forming cyanobacterium *Anabaena* sp. strain PCC 7120. *J Bacteriol* **196**, 4026–4035.
- 40 Kieninger AK, Forchhammer K & Maldener I (2019) A nanopore array in the septal peptidoglycan hosts gated septal junctions for cell-cell communication in multicellular cyanobacteria. *Int J Med Microbiol* **309**, 151303.
- 41 Bornikoel J, Carrión A, Fan Q, Flores E, Forchhammer K, Mariscal V, Mullineaux CW, Perez R, Silber N, Wolk CP *et al.* (2017) Role of two cell wall amidases in septal junction and nanopore formation in the multicellular cyanobacterium *Anabaena* sp. PCC 7120. *Front Cell Infect Microbiol* **7**, 386.
- 42 Springstein BL, Woehle C, Weissenbach J, Helbig AO, Dagan T & Stucken K (2020) Identification and characterization of novel filament-forming proteins in cyanobacteria. *Sci Rep* **10**, 1894.
- 43 Marchler-Bauer A, Bo Y, Han L, He J, Lanczycki CJ, Lu S, Chitsaz F, Derbyshire MK, Geer RC & Gonzales NR (2016) CDD/SPARCLE: functional classification of proteins via subfamily domain architectures. *Nucleic Acids Res* **45**, D200–D203.
- 44 Weissenbach J, Ilhan J, Bogumil D, Hülder N, Stucken K & Dagan T (2017) Evolution of chaperonin gene duplication in Stigonematalean cyanobacteria (subsection V). *Genome Biol Evol* **9**, 241–252.
- 45 Köster S, Weitz DA, Goldman RD, Aebi U & Herrmann H (2015) Intermediate filament mechanics in vitro and in the cell: from coiled coils to filaments, fibers and networks. *Curr Opin Cell Biol* **32**, 82–91.
- 46 Du Y, Cai Y, Hou S & Xu X (2012) Identification of the HetR recognition sequence upstream of hetZ in *Anabaena* sp. strain PCC 7120. *J Bacteriol* **194**, 2297–2306.
- 47 Solovyev V & Salamov A (2011) Automatic annotation of microbial genomes and metagenomic sequences. In *Metagenomics and its Applications in Agriculture, Biomedicine and Environmental Studies* (Li RW, ed.), pp. 61–78. Nova Science Publishers Inc., Hauppauge, NY.
- 48 Sakr S, Thyssen M, Denis M & Zhang CC (2006) Relationship among several key cell cycle events in the developmental cyanobacterium *Anabaena* sp. strain PCC 7120. *J Bacteriol* **188**, 5958–5965.
- 49 Springstein BL, Arévalo S, Helbig AO, Herrero A, Stucken K, Flores E & Dagan T (2020) A novel septal protein of multicellular heterocystous cyanobacteria is associated with the divisome. *Mol Microbiol* **113**, 1140–1154.
- 50 Wilson CGM, Magliery TJ & Regan L (2004) Detecting protein-protein interactions with GFP-fragment reassembly. *Nat Methods* **1**, 255–262.
- 51 Fenton AK, El ML, Lau DTC, Rudner DZ & Bernhardt TG (2016) CozE is a member of the MreCD complex that directs cell elongation in *Streptococcus pneumoniae*. *Nat Microbiol* **2**, 1–9.
- 52 Rojas ER & Huang KC (2018) Regulation of microbial growth by turgor pressure. *Curr Opin Microbiol* **42**, 62–70.
- 53 Yang Y, Huang X-Z, Wang L, Risoul V, Zhang C-C & Chen W-L (2013) Phenotypic variation caused by variation in the relative copy number of pDU1-based plasmids expressing the GAF domain of Pkn41 or Pkn42 in *Anabaena* sp. PCC 7120. *Res Microbiol* **164**, 127–135.
- 54 Flores E, Pernil R, Muro-Pastor AM, Mariscal V, Maldener I, Lechno-Yossef S, Fan Q, Wolk CP & Herrero A (2007) Septum-localized protein required for filament integrity and diazotrophy in the heterocyst-forming cyanobacterium *Anabaena* sp. strain PCC 7120. *J Bacteriol* **189**, 3884–3890.
- 55 Cho YW, Gonzales A, Harwood TV, Huynh J, Hwang Y, Park JS, Trieu AQ, Italia P, Pallipuram VK & Risser DD (2017) Dynamic localization of HmpF regulates type IV pilus activity and directional motility in the filamentous cyanobacterium *Nostoc punctiforme*. *Mol Microbiol* **106**, 252–265.
- 56 Kelemen GH (2017) Intermediate filaments supporting cell shape and growth in bacteria. In *Prokaryotic Cytoskeletons: Filamentous Protein Polymers Active in the Cytoplasm of Bacterial and Archaeal Cells* (Löwe J & Amos LA, eds), pp. 161–211. Springer International Publishing, Cham.
- 57 Lutkenhaus J (2012) The ParA/MinD family puts things in their place. *Trends Microbiol* **20**, 411–418.
- 58 Mullineaux CW, Mariscal V, Nenninger A, Khanum H, Herrero A, Flores E & Adams DG (2008) Mechanism of intercellular molecular exchange in heterocyst-forming cyanobacteria. *EMBO J* **27**, 1299–1308.

- 59 Daniel RA & Errington J (2003) Control of cell morphogenesis in bacteria: two distinct ways to make a rod-shaped cell. *Cell* **113**, 767–776.
- 60 Yang R, Bartle S, Otto R, Rogers M, Plamann L, Hartzell PL & Stassinopoulos A (2004) AglZ is a filament-forming coiled-coil protein required for adventurous gliding motility of *Myxococcus xanthus*. *J Bacteriol* **186**, 6168–6178.
- 61 England P, Bourhy P, Picardeau M, Saint Girons I, Mazouni K & Pehau-Arnaudet G (2005) The Scc spirochetal coiled-coil protein forms helix-like filaments and binds to nucleic acids generating nucleoprotein structures. *J Bacteriol* **188**, 469–476.
- 62 Ingerson-Mahar M, Briegel A, Werner JN, Jensen GJ & Gitai Z (2010) The metabolic enzyme CTP synthase forms cytoskeletal filaments. *Nat Cell Biol* **12**, 739–746.
- 63 Kühn J, Briegel A, Mörschel E, Kahnt J, Leser K, Wick S, Jensen GJ & Thanbichler M (2010) Bactofilins, a ubiquitous class of cytoskeletal proteins mediating polar localization of a cell wall synthase in *Caulobacter crescentus*. *EMBO J* **29**, 327–339.
- 64 Shieh Y-W, Minguez P, Bork P, Auburger JJ, Guilbride DL, Kramer G & Bukau B (2015) Operon structure and cotranslational subunit association direct protein assembly in bacteria. *Science* **350**, 678–680.
- 65 Bermudes D, Hinkle G & Margulis L (1994) Do prokaryotes contain microtubules? *Microbiol Rev* **58**, 387–400.
- 66 Jensen TE & Ayala RP (1980) Microtubule-like inclusions in isolates of the blue-green bacteria *Anabaena* and *Nostoc*. *Cytologia* **45**, 315–326.
- 67 Camargo S, Picossi S, Corrales-Guerrero L, Valladares A, Arévalo S & Herrero A (2019) ZipN is an essential FtsZ membrane tether and contributes to the septal localization of SepJ in the filamentous cyanobacterium *Anabaena*. *Sci Rep* **9**, 1–15.
- 68 Savage DF, Afonso B, Chen AH & Silver PA (2010) Spatially ordered dynamics of the bacterial carbon fixation machinery. *Science* **327**, 1258–1261.
- 69 Schumacher D & Sogaard-Andersen L (2017) Regulation of cell polarity in motility and cell division in *Myxococcus xanthus*. *Annu Rev Microbiol Regul* **71**, 61–78.
- 70 Typas A, Banzhaf M, Gross CA & Vollmer W (2012) From the regulation of peptidoglycan synthesis to bacterial growth and morphology. *Nat Rev Microbiol* **10**, 123–136.
- 71 Leung CL, Green KJ & Liem RKH (2002) Plakins: a family of versatile cytolinker proteins. *Trends Cell Biol* **12**, 37–45.
- 72 Birchler JA, Bhadra U, Bhadra MP & Auger DL (2001) Dosage-dependent gene regulation in multicellular eukaryotes: implications for dosage compensation, aneuploid syndromes, and quantitative traits. *Dev Biol* **234**, 275–288.
- 73 Persat A, Nadell CD, Kim MK, Ingremeau F, Siryaporn A, Drescher K, Wingreen NS, Bassler BL, Gitai Z & Stone HA (2015) The mechanical world of bacteria. *Cell* **161**, 988–997.
- 74 Park A, Jeong H-H, Lee J, Kim KP & Lee C-S (2011) Effect of shear stress on the formation of bacterial biofilm in a microfluidic channel. *BioChip J* **5**, 236–241.
- 75 Claessen D, Rozen DE, Kuipers OP, Sogaard-Andersen L & Van Wezel GP (2014) Bacterial solutions to multicellularity: a tale of biofilms, filaments and fruiting bodies. *Nat Rev Microbiol* **12**, 115–124.
- 76 Flärdh K, Richards DM, Hempel AM, Howard M & Buttner MJ (2012) Regulation of apical growth and hyphal branching in *Streptomyces*. *Curr Opin Microbiol* **15**, 737–743.
- 77 Young KD (2006) The selective value of bacterial shape. *Microbiol Mol Biol Rev* **70**, 660–703.
- 78 Singh SP & Montgomery BL (2011) Determining cell shape: adaptive regulation of cyanobacterial cellular differentiation and morphology. *Trends Microbiol* **19**, 278–285.
- 79 Lupas A, Van Dyke M & Stock J (1991) Predicting coiled coils from protein sequences. *Science* **252**, 1162–1164.
- 80 Boratyn GM, Schäffer AA, Agarwala R, Altschul SF, Lipman DJ & Madden TL (2012) Domain enhanced lookup time accelerated BLAST. *Biol Direct* **7**, 12.
- 81 Altschul SF, Gish W, Miller W, Myers EW & Lipman DJ (1990) Basic local alignment search tool. *J Mol Biol* **215**, 403–410.
- 82 Sonnhammer EL, von Heijne G & Krogh A (1998) A hidden Markov model for predicting transmembrane helices in protein sequences. *Proc Int Conf Intell Syst Mol Biol* **6**, 175–182.
- 83 Zhang Y (2009) I-TASSER: fully automated protein structure prediction in CASP8. *Proteins* **77**, 100–113.
- 84 Svetlitsky D, Dagan T & Ziv-Ukelson M (2020) Discovery of multi-operon colinear syntenic blocks in microbial genomes. *Bioinformatics* **36** (Suppl 1), i21–i29.
- 85 Ungerer J & Pakrasi HB (2016) Cpf1 is a versatile tool for CRISPR genome editing across diverse species of cyanobacteria. *Sci Rep* **6**, 1–9.
- 86 Wolk CP, Cai Y, Cardemil L, Flores E, Hohn B, Murry M, Schmetterer G, Schrautemeier B & Wilson R (1988) Isolation and complementation of mutants of *Anabaena* sp. strain PCC 7120 unable to grow aerobically on dinitrogen. *J Bacteriol* **170**, 1239–1244.
- 87 Cai Y & Wolk CP (1990) Use of a conditionally lethal gene in *Anabaena* sp. strain PCC 7120 to select for double recombinants and to entrap insertion sequences. *J Bacteriol* **172**, 3138–3145.
- 88 Mohr R, Voß B, Schliep M, Kurz T, Maldener I, Adams DG, Larkum ADW, Chen M & Hess WR (2010) A new chlorophyll d-containing cyanobacterium:

- evidence for niche adaptation in the genus *Acaryochloris*. *ISME J* **4**, 1456–1469.
- 89 Fiedler G, Arnold M, Hannus S & Maldener I (1998) The DevBCA exporter is essential for envelope formation in heterocysts of the cyanobacterium *Anabaena* sp. strain PCC 7120. *Mol Microbiol* **27**, 1193–1202.
- 90 Nieves-Mori3n M, Lechno-Yossef S, L3pez-Igual R, Fr3as JE, Mariscal V, N3rnberg DJ, Mullineaux CW, Wolk CP & Flores E (2017) Specific glucoside transporters influence septal structure and function in the filamentous, heterocyst-forming cyanobacterium *Anabaena* sp. strain PCC 7120. *J Bacteriol* **199**, e00876-16.
- 91 Lehner J, Berendt S, D3rsam B, P3rez R, Forchhammer K & Maldener I (2013) Prokaryotic multicellularity: a nanopore array for bacterial cell communication. *FASEB J* **27**, 2293–2300.
- 92 Rudolf M, Tetik N, Ramos-Le3n F, Flinner N, Ngo G, Stevanovic M, Burnat M, Pernil R, Flores E & Schleiff E (2015) The peptidoglycan-binding protein SjcF1 influences septal junction function and channel formation in the filamentous cyanobacterium *Anabaena*. *MBio* **6**, e00376-15.
- 93 Schneider CA, Rasband WS & Eliceiri KW (2012) NIH Image to ImageJ: 25 years of image analysis. *Nat Methods* **9**, 671.
- 94 Karimova G, Davi M & Ladant D (2012) The β -lactam resistance protein Blr, a small membrane polypeptide, is a component of the *Escherichia coli* cell division machinery. *J Bacteriol* **194**, 5576–5588.
- 95 Camberg JL, Hoskins JR & Wickner S (2009) ClpXP protease degrades the cytoskeletal protein, FtsZ, and modulates FtsZ polymer dynamics. *Proc Natl Acad Sci USA* **106**, 10614–10619.
- 96 Urrejola C, von Dassow P, van den Engh G, Salas L, Mullineaux CW, Vicu3a R & Sanchez-Baracaldo P (2020) Loss of filamentous multicellularity in cyanobacteria – the extremophile *Gloeocapsopsis* sp. strain UTEX B3054 retained multicellular features at the genomic and behavioral levels. *J Bacteriol* **202**, e00514-19.
- 97 Ramos-Le3n F, Mariscal V, Battchikova N, Aro EM & Flores E (2017) Septal protein SepJ from the heterocyst-forming cyanobacterium *Anabaena* forms multimers and interacts with peptidoglycan. *FEBS Open Bio* **7**, 1515–1526.

Supporting information

Additional supporting information may be found online in the Supporting Information section at the end of the article.

Fig. S1. *zicK* and *zacK* are expressed at standard growth conditions.

Fig. S2. *In vitro* polymerization assay controls.

Fig. S3. Co-polymerization of ZicK and ZacK is dosage-dependent.

Fig. S4. Ectopic expression of ZicK and ZacK.

Fig. S5. Host-independent heteropolymerization of ZicK and ZacK upon heterologous expression in *E. coli*.

Fig. S6. Complementation of the zigzagged growth phenotype of the $\Delta zicK\Delta zacK$ mutant and its ability to grow under diazotrophic conditions.

Fig. S7. ZicK and ZacK do not interact with other components of the septal junctions besides SepJ.

Fig. S8. The $\Delta zicK\Delta zacK$ mutant is not defective in intercellular transport and cellular ultrastructures.

Fig. S9. PG biogenesis and Z-ring placement are largely unaffected in the $\Delta zicK\Delta zacK$ mutant.

Table S1. Cyanobacterial strains.

Table S2. *E. coli* strains.

Table S3. Plasmids.

Table S4. Oligonucleotides.